

## THERMAL PROPERTY DATABASE FOR INVESTMENT CASTING SHELLS

Mingzhi Xu, Simon N. Lekakh, and Von L. Richards  
Missouri University of Science and Technology, Rolla, MO, USA

Copyright © 2016 American Foundry Society  
DOI 10.1007/s40962-016-0052-4

### Abstract

Reliable and realistic thermal properties data for investment casting shell molds are required to correctly simulate the solidification and predict the shrinkage. Investment casting shells exhibit several phase transformations during firing and pouring which affect their transient thermal properties. These properties are dependent upon time, temperature and process history. This study presents the thermal properties (thermal conductivity and specific heat capacity) of seven industrially produced ceramic molds using an inverse method in which pure Ni was poured into ceramic molds equipped with two thermocouples (inside the mold cavity and in the shell). MAGMASOFT<sup>®</sup> software

(hereafter known as Software A) was used to simulate virtual cooling curves which were fitted to experimental curves by adjusting the temperature dependent thermal properties of the ceramic mold. The thermal properties data obtained from the inverse method were compared with measurement results from laser flash and the differences were discussed. The dataset thus developed will serve to improve the accuracy of investment casting simulation.

**Keywords:** investment casting, thermal property, inverse method, laser flash, database

### Introduction

Steel casting solidification in an investment ceramic shell is affected by thermal properties of the shell, including thermal conductivity and specific heat capacity. In a relatively thin-walled casting [5–15 mm (0.2–0.6 in.)], most super heat and part of the latent heat of the liquid metal are accumulated in the shell, where specific heat capacity plays an important role. However, the excessive heat from massive casting will transfer through the shell in which cases thermal conductivity is predominant. Both of these two factors (heat accumulation and heat transfer) are significant in order to have representative simulations for industrial use to control shrinkage defects and optimize casting quality.

Because of the wide variety of shell compositions, particle size distribution, and processing parameters, the ceramic

shell could have from ten to thirty percent porosity,<sup>1</sup> which can provide air permeability but also has a strong effect on the mechanical and thermal properties of the shell.<sup>2–4</sup> In the general case, the effect of porosity on the thermal conductivity of ceramic media can be estimated using Eqn. 1.<sup>5</sup>

$$k_r = \exp(-1.5\varphi/(1 - \varphi)) \quad \text{Eqn. 1}$$

where  $\varphi$  is the porosity, and  $k_r = k/k_0$  is the relative thermal conductivity, with  $k$  denoting the effective thermal conductivity of the porous material and  $k_0$  denoting the thermal conductivity of the dense solid material.

Thermal processing history also influences the shell thermal properties. There are several thermal history stages involved in the entire process, including pattern removal/de-waxing [80–300 °C (176–572 °F)]; sintering/firing [600–1000 °C (1112–1832 °F)]; preheating [800–1200 °C (1472–2192 °F)] and pouring [1500–1600 °C (2732–2912 °F)]. Colloidal silica binder as well as flour/filler and often ceramic stucco have amorphous structure at significant extent. The degree to which the amorphous to crystalline transformation takes place during different thermal history conditions affects the thermal properties of the shell.<sup>6</sup>

A version of this paper was previously published in 2014 AFS Transactions.

The transient nature of the thermal properties of investment shells make it difficult to precisely measure them, using classical methods which require steady state conditions. Huang et al.<sup>7</sup> measured the thermal conductivity of investment casting ceramic components by using the hot wire method, but they obtained the data for pure materials used in investment casting processing and not the composite shell structure. Additionally, the hot wire method requires a relatively large isotropic sample, which is only applicable for shells made of multiple coats of the same type of materials and does not consider the layered structure of real ceramic shells.<sup>8</sup> Connolly et al.<sup>9</sup> measured the specific heat capacity of investment casting shells prepared from a slurry consisting of a 3.7:1 (by weight) mixture of zircon and silica in an aqueous colloidal silica binder using differential scanning calorimetry (DSC) but the mixture did not represent industrially sized porous shell. Konrad<sup>10</sup> and Mahimkar<sup>4</sup> measured the thermal diffusivity of the shell using the laser flash method, which was designed for an ideally dense specimen with uniform thickness. The open pores on the surface of the shell introduce an inconsistency in the data interpretation. To counter this distortion, Garcia<sup>11</sup> suggested attaching two thin copper disks to a porous specimen to ensure a known effective thickness. However this method is not applicable for a brittle investment ceramic shell.

With the difficulties in directly measuring the thermal property of the non-uniform porous shell, the inverse method, which characterizes the thermal properties of the bulk shell during the real casting process, is used. In this case, a shell mold with installed thermocouples is poured with a pure liquid metal, which has well defined properties. Shell thermal properties are estimated by running multiple computational fluid dynamic (CFD) simulation iterations, varying the thermal conductivity and specific heat capacity over a range of values in an effort to fit the calculated cooling curves to the experimental cooling curves for the shell and casting.<sup>12,13</sup> However, the inverse method takes much effort to get an acceptable fit among those curves. Sabau and Viswanathan<sup>8</sup> studied thermo-

physical properties of zircon and fused silica based investment casting shells using the inverse method. They measured thermal diffusivity ( $\alpha$ ) of zircon based prime coat and generated  $C_p$  and coefficient of thermal conductivity ( $K$ ) data from it.

In this paper, the author introduces a method to correct the specimen thickness used in the laser flash method, in order to obtain more accurate thermal property data. Afterwards, those physically measured thermal property data are applied to the inverse method as the starting points to reduce a significant amount of computational time and avoid errors, induced from extrapolation in the optimization algorithm. Seven industrial shells are evaluated. Thermal property database are developed to help increase the accuracy of the investment casting simulations.

## Design of Experiments

### Pattern and Shell

A 76.2 × 76.2 × 25.4 mm (3 × 3 × 1 in.) expandable polystyrene (EPS) foam pattern, attached to a pouring cup, was used in this study. Patterns were sent to several industrial foundries for shelling. Pattern removal, firing and properties analyses were done at Missouri University of Science and Technology. Shells were pre-fired according to requirements from each individual foundry. Seven different industrial shells were built using the aqueous colloidal silica binder with different mineral fillers as listed in Table 1.

### Improved Laser Flash Method

In a laser flash thermal diffusivity test, a small specimen is subjected to a high intensity short duration radiant laser pulse after thermal equilibration at the test temperature of interest. Typical specimen disc dimensions are 12.7 mm (0.5 in.) square by 2 mm (0.07 in.) thickness. The energy of the pulse is absorbed on the front surface of the specimen

**Table 1. Composition of Industrial Shells Used in This Study**

	Prime coat		Backup coat		Seal coat Slurry	Firing temperature, °C
	Slurry	Stucco	Slurry	Stucco		
Shell #1	Fused silica + zircon	Fused silica	Fused silica	Fused silica	Fused silica	850
Shell #2	Fused silica + zircon	Zircon	Fused silica	Fused silica	Fused silica	982
Shell #3	Fused silica					850
Shell #4	Alumina + silica					850
Shell #5	Alumina					850
Shell #6	Fused silica + zircon	Aluminosilicate	Aluminosilicate + fused silica	Aluminosilicate + fused silica	Aluminosilicate + fused silica	850
Shell #7	Zircon + aluminosilicate (rapid shelling process)					850

and the resulting rear face temperature rise is recorded by a non-contact infrared radiation thermometer. The thermal diffusivity ( $\alpha$ ) is calculated<sup>14</sup> from specimen thickness ( $L$ ) and time ( $t_{1/2}$ ) required for rear face temperature to reach 50 % of its maximum value (Eqn. 2):

$$\alpha = 0.1388L^2/t_{1/2} \quad \text{Eqn. 2}$$

In differential laser flash calorimetry, a reference specimen (graphite, subscript “R”) and the test specimen (shell, subscript “M”) are mounted together under the same condition at the same temperature and irradiated uniformly with homogenized laser beam. To insure similar emissivity, graphite spray coating is used to cover the front and rear faces of both the reference and the test specimens. The temperature rise ( $\Delta T$ ) of the reference with known specific heat capacity ( $C_p$ ) and the specimen are measured. If the density ( $\rho$ ) of the shell is known then specific heat capacity of the shell can be calculated (Eqn. 3):

$$(\rho c_p)_M = \frac{L_R \Delta T_R}{L_M \Delta T_M} (\rho c_p)_R \quad \text{Eqn. 3}$$

Finally, thermal conductivity ( $K$ ) of the shell can be calculated by substituting measured value of specific heat capacity along with the thermal diffusivity in (Eqn. 4):

$$K = \rho C_p \alpha \quad \text{Eqn. 4}$$

As discussed in another published paper,<sup>15</sup> the laser flash method, previously mentioned, was designed for dense specimens, while measurement of highly porous materials has associated difficulties in defining the applicable specimen thickness,  $L$ , used in Eqn. 2. To evaluate the effective specimen thickness and density, the author used a three-dimensional high resolution optical profiler to obtain the specimen surface topology (Figure 1). Then the effective thickness,  $L_{ef}$  and density were determined and these data were used in Eqns. 2 and 3. Samples were put into an ambient furnace with 15 °C (27 °F)/min heating rate and laser flash tested from 200 °C (392 °F) to 1200 °C (2192 °F) at intervals of 200 °C (360 °F) after a 10 min holding time at each measurement temperature.

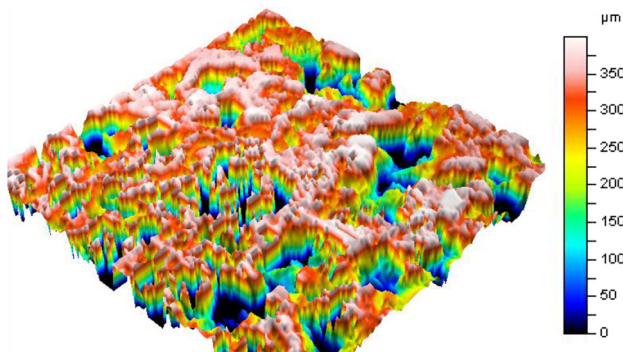


**Figure 1. Surface topology is used to calculate the effective thickness of specimen.**

Specimens were taken separately from prime coats and backup coats. For comparison, the rule of mixtures was used to estimate the thermal property of the entire shell based on the thickness ratio between the prime coats and backup coats. Three runs of each type of specimen were conducted and the average values are reported in the results.

### Inverse Method: Experimental Setup and Simulation

After firing the shells, one S-type thermocouple [protected by a 2 mm (0.08 in.) diameter OD quartz sheath] was installed in the center of the mold cavity, and the other K-type thermocouple was buried 1 mm (0.04 in.) below the external shell surface, at the same casting height with the S-type thermocouple. The shells were then entirely wrapped with 12.7 mm (0.5 in.) thick insulation (aluminosilicate fiber, Durablanket S, 8 pcf), to thermally isolate the shell and limit the influence of the external cooling environment. The shell was then poured with pure nickel (99.5 % Ni) at an initial pouring temperature about 1520 °C (2768 °F) A 24-bit data acquisition system was used to collect the temperature curves.

CFD inverse modeling was done using the optimization module of Software A. Initially, a base simulation was completed that would represent the actual casting conditions as closely as possible using initial properties. The processing information for initial shell and liquid metal temperatures, pouring time and insulating wrap locations were used in the simulation definition (Figure 2). The nickel dataset was created from the known pure nickel data (Table 2).<sup>16</sup> Initially, property dataset measured by laser flash was used as a starting point. An insulating wool dataset was obtained from thermo-physical data available in the product datasheet.<sup>17</sup> The heat transfer coefficient (HTC) assumed between the casting and shell was 3500 W/m<sup>2</sup> K (HTC1) and between the shell and insulating wool was 1000 W/m<sup>2</sup> K (HTC2).<sup>18</sup> These values of heat transfer

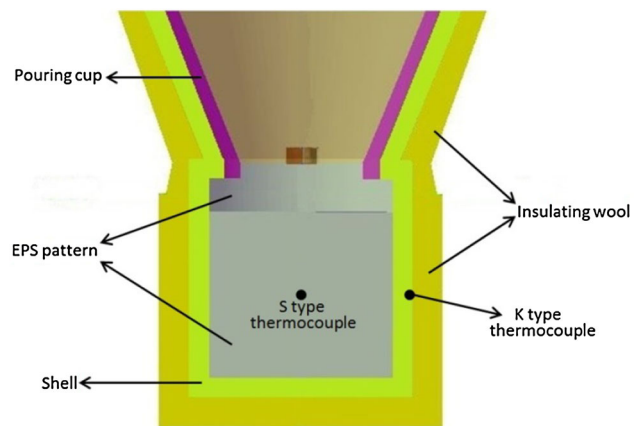


**Figure 2. This is a schematic of pattern and ceramic investment casting shell mold.**

**Table 2. Properties of Pure Nickel Used for Inverse Modeling**

$C_p$ , J/g K		Latent heat, J/g	$T_s$ , °C	Density, g/cm <sup>3</sup>		$K$ , W/m K		
Solid	Liquid			Solid	Liquid	Solid	Liquid	
$(1.62 \times 10^{-4}) \times T, \text{°C} + 0.427$		0.734	279.9	1455	7.9	7.8	80	60

coefficients assumed that there were no significant additional boundary thermal ceramic shell and the casting would not have a significant resistances. For example, any air gap between the effect due to the predominance of radiant heat transfer and the large difference in thermal diffusivity between the shell and the metal.

The goal for the inverse method was to achieve computationally simulated curves which were well-fitted to the experimentally measured curves of temperatures. This fitting would be achieved through the definition of objectives and design variables. The initial simulation setup described was the baseline for the initial curve to be compared with the temperature curves obtained from the experimental castings. The curve mismatch was defined in the optimization using two methods: (1) Riemann error and (2) specified gradient error.<sup>19</sup> The Riemann error term utilizes the absolute area between the two curves, which defines how far the two curves are apart over the entire duration. The specified gradient error term compares the slope of the curves by comparing the difference of the vector angle representation of the slope of segments between base points on both the simulated and measured curves, which will describe how well the shapes of the curves match. The objectives were to minimize the values for both. Figure 3 shows an example of the good match between calculated and experimental temperature curves after hundreds of simulations.

The specific heat capacities and thermal conductivity of the shell and insulating material as well as external heat

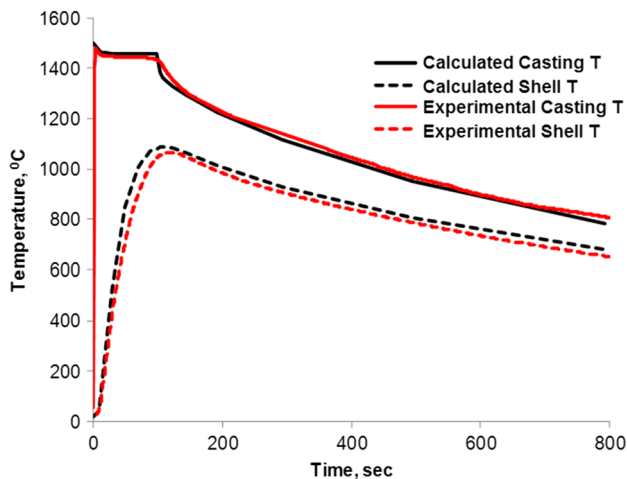


**Figure 3. Graph shows the inverse calculated thermal curves after optimization fitted to experimentally obtained results.**

transfer coefficient (HTC3) are the main parameters that influence the temperature curves of the casting and the shell. Preliminary modeling showed that solidification time and the coordinates of the point where the shell reached the highest temperature were mainly influenced by the specific heat capacity and thermal conductivity of the shell. For higher  $C_p$  of the shell, more energy is needed to heat up the shell to a certain temperature. Thus, the solidification time will be shorter. Higher  $K$  of the shell will allow the heat of the liquid metal to flow through the shell more quickly, which also shortens the solidification time and increases the maximum temperature of the shell. Sensitivity testing by modeling also showed that the external heat transfer coefficient HTC3 mainly affected the shell and casting cooling rates after solidification was completed. The thermal property dataset, giving the best match between those curves, will be presented subsequently and the differences between the data from the inverse method and the data from the laser flash method will be discussed.

### Density and Porosity

To evaluate the shell density and porosity, whole pieces of the shell containing all layers were examined. Archimedes method<sup>20</sup> was used to calculate the overall bulk density and open porosity accessible for water. In addition, a shell specimen was crushed to 100 mesh and *He*-pycnometer was used to obtain the theoretical density. Because helium gas has little restriction of penetration into small size pores, the effect of closed porosity was eliminated. Then the total porosity and closed porosity were calculated.

### Results

Table 3 shows the densities and porosities of the seven industrial shells after pre-firing at 850 °C (1562 °F) for one hour. The silica-based shells (#1, #3) are less dense compared with the aluminosilicate-based shells (#4, #6). The alumina-based shells (#5) have the highest density among these industrial shells. Total porosity mostly depends on the shell-building process (particle sizes, slurry viscosity etc.), but it was observed that shell #7, made by a rapid shelling process, is almost 40 % porous.

### Thermal Properties from Inverse Method

Figure 4 shows the specific heat capacity and thermal conductivity data estimated by the inverse method. Data

**Table 3. Densities and Porosities of Industrial Shells Used in this Study**

	Bulk density, g/cm <sup>3</sup>	Theoretical density, g/cm <sup>3</sup>	Open porosity, %	Closed porosity, %	Total porosity, %
Shell #1	1.64	2.41	21.7	10.0	31.7
Shell #2	1.53	–	25.7	–	–
Shell #3	1.63	2.42	23.0	9.9	32.9
Shell #4	1.93	2.90	23.8	9.7	33.5
Shell #5	2.24	3.30	21.0	11.1	32.1
Shell #6	1.98	3.18	26.1	11.6	37.7
Shell #7	1.96	3.26	26.7	13.1	39.8

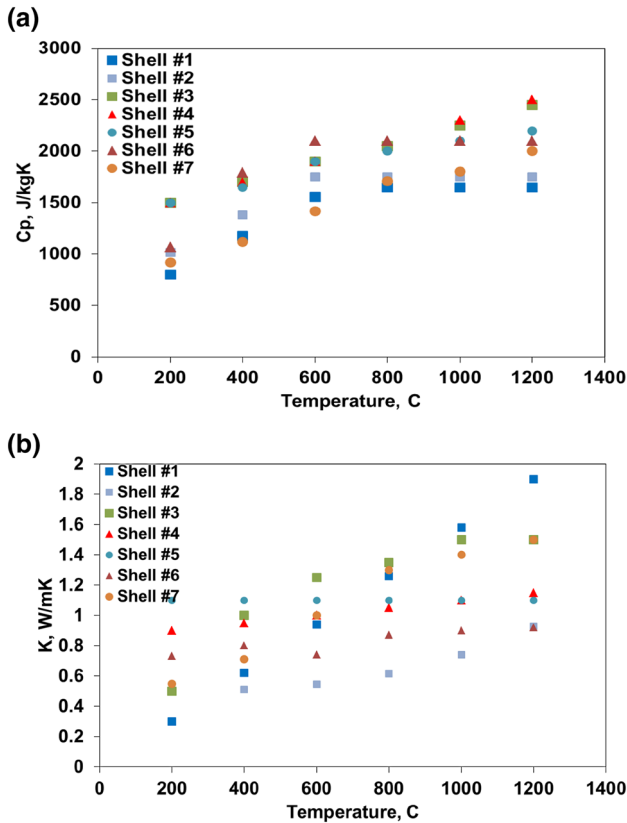


**Figure 4. Graphs show (a) specific heat capacity and (b) thermal conductivity values of studied shells determined by the inverse method.**

are summarized in Table 5 in the “Appendix”. Temperature dependent specific heat capacities in all shells had a similar trend, but the average and maximum values mainly depend on the phase of starting materials and the reactions and transformations during the thermal processing, which were not readily predictable.

Generally, at above room temperature, the thermal conductivity of most dense ceramics decreases with increasing temperature because phonon scattering is more intense from the vibrating lattice at a higher temperature. However, the investment casting shells, where the colloidal silica is used as a binder in most cases and a significant amount of fused silica is utilized as flour and stucco, more often show

an increasing thermal conductivity at higher temperatures due to the photon radiation becoming dominant at higher temperature in semi-transparent silica.

Porosity has a significant influence on the thermal conductivity. Between the two aluminosilicate shells (#4 and #6), #6 with higher total porosity (37.65 %) exhibited lower thermal conductivity values throughout the measured temperature range compared to shell #4 having lower total porosity (33.52 %).

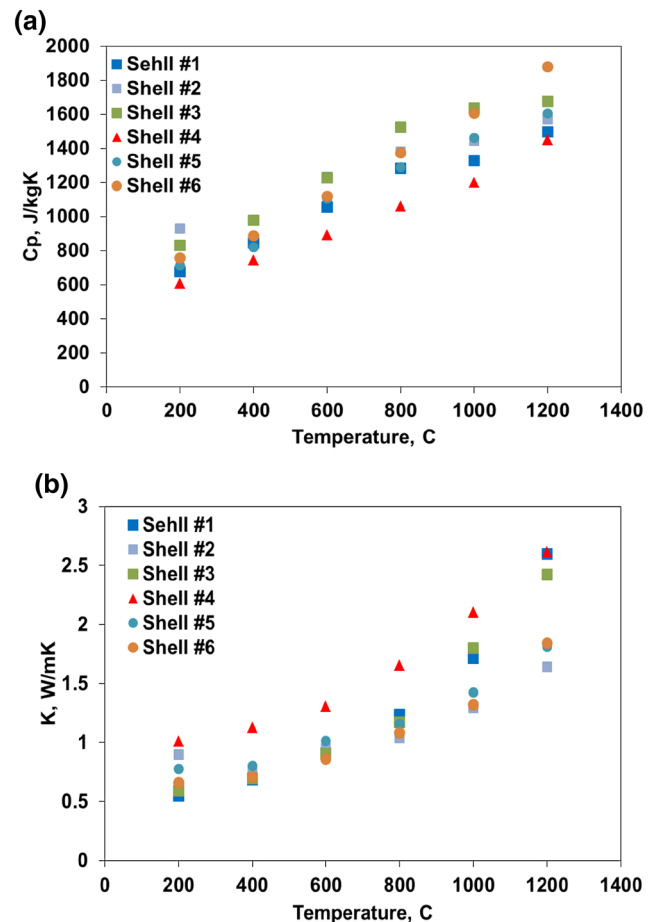


**Figure 5. Graphs show (a) specific heat capacity and (b) thermal conductivity values of the shells studied and determined by the improved laser flash method.**



Another good example is the weak temperature dependence of conductivity in the alumina based shell (#5). Since the photon radiation in alumina is not significant until 1000 °C (1832 °F), this radiation compensates phonon scattering in alumina and the porosity effects and consequently the thermal conductivity didn't change much over the elevated temperature range.

### Thermal Properties from Laser Flash

The thermal conductivity and specific heat capacity values measured from laser flash for the shells studied are listed in Figure 5. Shell #7 (rapid shelling technique) was highly porous and broke apart when being surface ground during laser flash sample preparation. Effective density calculated from sample surface topography was used to calculate these values. It was found that laser flash showed a similar

trend to the inverse method on both thermal conductivity and heat capacity values.

### Discussion

#### Comparison among Inverse Method, Laser Flash and Theoretical Values

When putting thermal property data from inverse method and laser flash method together, as shown in Figure 6, it was observed that the thermal conductivity values were fairly close between those two methods, however the inverse method presented higher specific heat capacity values than the laser flash method. Because many thermal reactions among the shell components and phase transformation within the amorphous silica take place at high temperature,

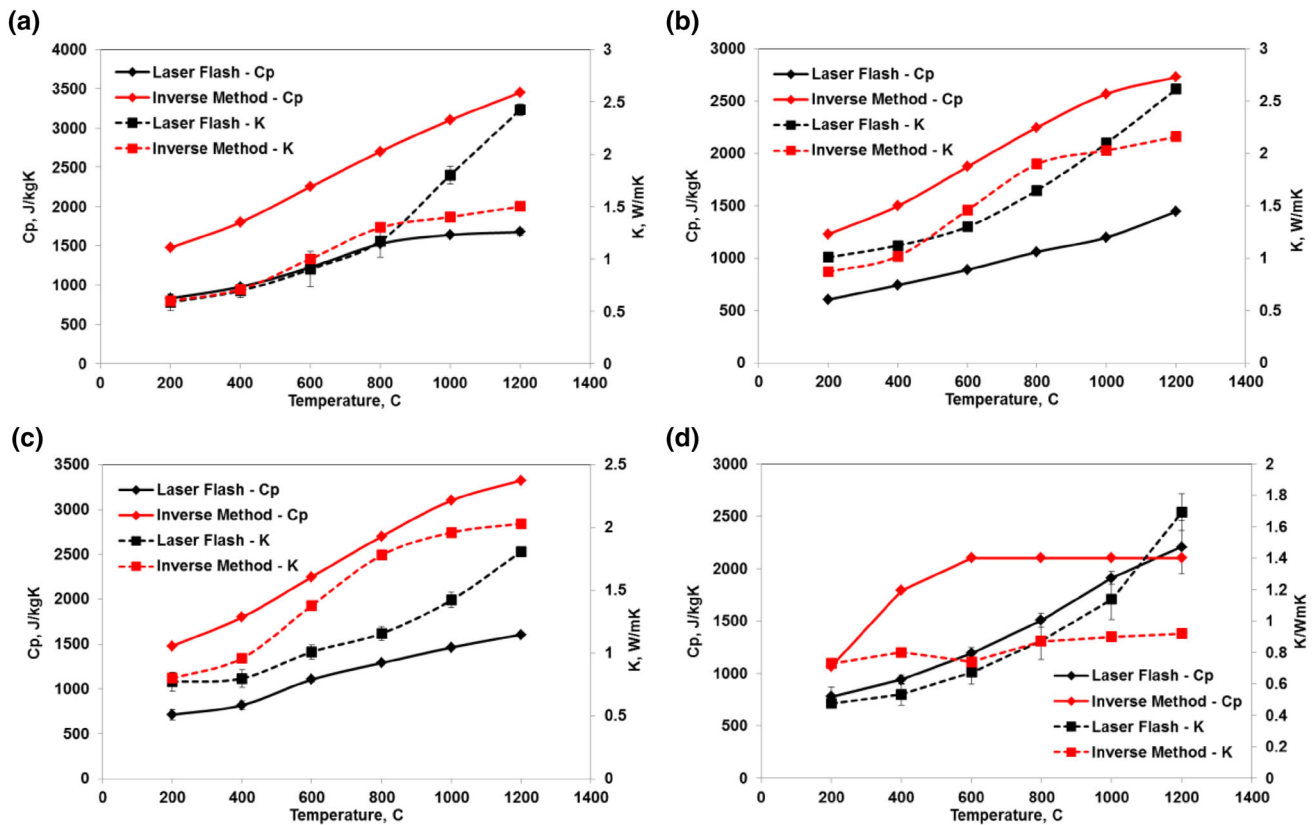


Figure 6. Graphs show the comparison of  $C_p$  and  $K$  values determined by the inverse and improved laser flash methods: (a) shell #3; (b) shell #4; (c), shell #5 and (d) shell #6.

Table 4. Total Reaction Enthalpy Change from 20 °C (68 °F) to 1420 °C (2588 °F), (J/g)

Thermal cycle from initial to final conditions	Theoretically calculated	From inverse method			From laser flash		
		Shell #1	Shell #2	Shell #3	Shell #1	Shell #2	Shell #3
Amorphous (20 °C) → Cristobalite (1420 °C)	1397.80	1917	2092	2791	1554	1731	1815
Cristobalite (1420 °C) → Cristobalite (20 °C)	1557.30						

the amount and rate of these reactions, i.e. sintering and devitrification, will significantly affect the effective  $C_p$  values used in modeling. In the inverse method, the shell is heated rapidly when metal is poured and shell is cooled down at a relatively slower cooling rate as the metal solidifies. These processes associate with more instantaneous measurements of a property which includes latent heat effects from phase changes. However, a small mass specimen is equilibrated at an environmental test temperature in the laser flash. Consequently, the transformation occurring in the inverse method may have already taken place prior to the measurement by the laser flash method.

Similarly, when comparing the total enthalpy change (Table 4) from room temperature, 20 °C (68 °F), to 1420 °C (2588 °F) among the values from theoretical calculation<sup>16</sup> of the inverse method and the laser flash method, the laser flash method shows similar total reaction enthalpy values to the theoretically calculated values; because the thin specimen used in the laser flash method was under partially thermally stabilized condition which is closer to thermal equilibrium. Nevertheless the shell in reality is hardly in thermal equilibrium conditions. Thus the inverse method provided more realistic effective heat capacity values for modeling the pouring and solidification processes. However, thermal property data measured from laser flash could be used as the starting points in the automatic optimization process, which greatly reduces the number of simulation cases needed to approach a well fitted case and reduces the potential extrapolation error in iteration step estimates.

Based on Eqn. 1, the theoretical thermal conductivity of pure silica<sup>21</sup> with 33 % porosity was plotted in Figure 7 as well as thermal conductivity values of shell #1 and shell #3. Those industrial shells had similar measured and theoretical values of thermal conductivity at a lower temperature [ $<400$  °C (752 °F)] but were more heat conductive at a higher temperature. This could result from different particle and porosity size distributions, since smaller particle size with higher grain boundary to volume ratio will lower the thermal conductivity. Moreover, this theoretical model may not consider the photon conductivity of the pore phase at higher temperature.

### Recommendations on Utilizing the Data

Obtaining the data from laser flash then applying the data in the inverse method can be time consuming and costly. It is recommended that industries, developing their own investment casting shells, can pick the thermal property

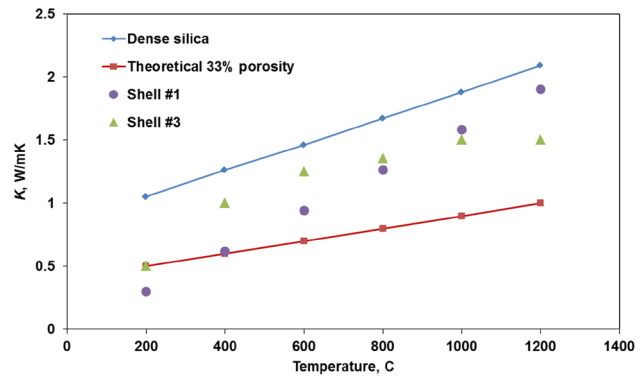


**Figure 7. Graph shows the comparison on thermal conductivity between theoretical values and inverse method results.**

data of shells from given foundries in this paper with the closest composition and utilize those in their simulations. Whoever uses these data needs to measure the bulk density and porosity of their shells, since bulk density is used in most of simulations and porosity is needed to adjust the value of thermal conductivity. Pre-firing temperature was proven to have some influence on the thermal properties, which will be discussed in a future publication.

### Conclusion

This paper introduced a method to allow laser flash method to reduce the measurement discrepancy due to open porosity of the sample by determining the effective thickness of the sample with the help of a 3D optical profiler. The inverse method was used to generate a realistic thermal property database of investment casting shell, which considers the phase transitions and reactions during the entire process. The differences and correlations between laser flash and inverse method were discussed.

The authors presented an effective and relatively accurate way to determine the thermal property data of investment casting shells containing metastable phases by using a combination of laser flash and inverse methods. Thermal property databases were developed for seven industrial shell systems and recommendations about utilizing the database for industrial simulation have been included.

### Appendix

See Table 5.

Table 5. Thermal Properties Data of Shells from Inverse Method (as Plotted in Figure 4)

Temp., °C	Shell 1		Shell 2		Shell 3		Shell 4		Shell 5		Shell 6		Shell 7	
	$C_p$ , J/kg K	$K$ , W/m K	$C_p$ , J/kg K	$K$ , W/m K	$C_p$ , J/kg K	$K$ , W/m K	$C_p$ , J/kg K	$K$ , W/m K	$C_p$ , J/kg K	$K$ , W/m K	$C_p$ , J/kg K	$K$ , W/m K	$C_p$ , J/kg K	$K$ , W/m K
200	800	0.30	1015	0.50	1500	0.50	1500	0.90	1500	1.10	1070	0.73	920	0.55
400	1175	0.62	1382	0.51	1700	1.00	1700	0.95	1650	1.10	1790	0.80	1120	0.71
600	1555	0.94	1750	0.55	1900	1.25	1900	1.00	1900	1.10	2100	0.74	1415	1.00
800	1650	1.26	1750	0.62	2050	1.35	2100	1.05	2000	1.10	2100	0.87	1710	1.30
1000	1650	1.58	1750	0.74	2250	1.50	2300	1.10	2100	1.10	2100	0.90	1800	1.40
1200	1650	1.90	1750	0.93	2450	1.50	2500	1.15	2200	1.10	2100	0.92	2000	1.50

## REFERENCES

1. D.M. Kline, S.N. Lekakh, V.L. Richards, K. Chandrashekhara, J. Chen, Stucco size comparison and simulated pressure loading of investment casting shells. *AFS Trans.* **117**, 341–353 (2009)
2. S. Ding, Y. Zeng, D. Jiang, Gas permeability behavior of mullite-bonded porous silicon carbide ceramics. *J. Mater. Sci.* **42**, 7171–7175 (2007)
3. T. Isobe, Gas permeability and mechanical properties of porous alumina ceramics with unidirectional aligned pores. *J. Eur. Ceram. Soc.* **27**, 53–59 (2007)
4. C. Mahimkar, V.L. Richards, S.N. Lekakh, in *High Temperature Thermo-Physical Properties of Ceramic Shell, 57th Annual Technical Meeting*. Investment Casting Institute (2010)
5. Z. Zivcova, E. Gregorova, W. Pabst, D. Smith, A. Michot, C. Poulhier, Thermal conductivity of porous alumina ceramics prepared using starch as a pore-forming agent. *J. Eur. Ceram. Soc.* **29**, 347–353 (2009)
6. G. Hart, The nomenclature of silica. *Am. Mineral.* **12**, 383–395 (1927)
7. H. Huang, J.T. Berry, X.Z. Zheng, T.S. Piwonka, in *Thermal Conductivity of Investment Casting Ceramics, 37th Annual Technical Meeting*. Investment Casting Institute (1989)
8. A.S. Sabau, S. Viswanathan, Thermo-physical properties of zircon and fused silica based shells for investment casting. *AFS Trans.* **112**, 649–661 (2004)
9. S. Connolly, S. Jones, P.M. Marquis, Specific heat of investment casting shell, in *Proceedings of the 10th World Conference on Investment Castings*, ed. by EICF (EICF, Monaco, 2000), pp. 8–9
10. C.H. Konrad, M. Brunner, K. Kyrgyzbaev, R. Völkl, U. Glatzel, Determination of heat transfer coefficient and ceramic mold material parameters for alloy IN738LC investment castings, in *Metals and Alloys* (University Bayreuth, Bayreuth, 2011)
11. E. Garcia, M.I. Osendi, P. Miranzo, Thermal diffusivity of porous cordierite ceramic burners. *J. Appl. Phys.* **92**(5), 2346–2349 (2002)
12. E. Majchrzak, Identification of cast steel latent heat by means of gradient method. *Int. J. Comput. Mater. Sci. Surf. Eng.* **1**(5), 555–570 (2007)
13. K.D. Carlson, C. Beckermann, Development of thermo-physical property datasets, benchmark Niyama results and a simulation qualification procedure, in *Proceeding of the 64th SFSA Technical and Operating Conference*, paper no. 5.5 (2010)
14. K. Shinzato, T. Baba, A laser flash apparatus for thermal conductivity and specific heat capacity measurements. *J. Therm. Anal. Calorim.* **64**, 413–422 (2001)
15. M. Xu, S.N. Lekakh, C. Mahimkar, V.L. Richards, S.A. Dutler, Measurements and confirmation of thermal properties of investment ceramic shell by multiple methods. *AFS Trans.* **120**, 229–236 (2012)



16. FactSage(TM) 6.2
17. *Unifrax Product Information Sheet, Form C-1421*, pp. 1–8 (2000)
18. J.W. Woolley, K.A. Woodbury, The interfacial heat transfer coefficient of metal castings—a literature review. *AFS Trans.* **115**, 1–18 (2007)
19. *MAGMASOFT® Version 4.4, MAGMAfrontier Module Manual*, pp. 6-88-99 (2005)
20. ASTM Standard C20, in *Standard Test Methods for Apparent Porosity, Water Absorption, Apparent Specific Gravity, and Bulk Density of Burned Refractory Brick and Shapes by Boiling Water* (ASTM International, West Conshohocken, PA, 2000). [www.astm.org](http://www.astm.org)
21. J.F. Shackelford, W. Alexander, in *CRC Practical Handbook of Materials Selection* (CRC Press, Boca Raton, FL, 1995), p. 404